Pergamon

Phys. Chem. Earth (B), Vol. 24, No. 3, pp. 177–185, 1999

1464-1909/99/$—see front matter

PII: S1464-1909(98)00034-3

Off-beam Lidar: an Emerging Technique in Cloud Remote Sensing Based on Radiative Green-function Theory in the Diffusion Domain

A. B. Davis[1], R. F. Cahalan[2], D. Spinehirne[3], M. J. McGill[3] and S. P. Love[1]

[1]Los Alamos National Laboratory, Nonproliferation and International Security Division, Space and Remote Sensing Sciences Group (NIS-2), P.O. Box 1663 (Mail Stop C-323), Los Alamos, NM 87545, U.S.A.
[2]NASA's Goddard Space Flight Center, Climate and Radiation Branch (Code 913), Greenbelt, MD 20771, U.S.A.
[3]NASA's Goddard Space Flight Center, Mesoscale Dynamics Branch (Code 912), Greenbelt, MD 20771, U.S.A.

Received 1 June 1998; revised 8 September 1998; accepted 1 October 1998

Abstract. Atmospheric lidars do not penetrate directly most boundary-layer clouds due to their large optical density. However, the lidar's photons are not absorbed but scattered out of the beam. Typically, about half are actually transmitted through the cloud and the other half escape the cloud by reflection in extended diffuse patterns that evolve in time. For all practical purposes, these are the cloud's space-time Green functions (GFs). In a Fourier-Laplace expansion of the space-time GF, the leading term is representative of solar remote-sensing (i.e., steady/uniform source) while higher-order terms correspond to active approaches with temporal- and/or spatial- resolution capabilities. Radiative GF theory is tractable within the limits of photon-diffusion theory and homogeneous clouds. Monte Carlo simulations with realistically variable cloud models are used to extend the range of validity of analytical GF theory with minor modifications. GF theory tells us that physical and optical cloud thicknesses can be retrieved from off-beam cloud lidar returns.

1 Introduction and Overview

Traditional ("on-beam") atmospheric lidar reveals little about boundary-layer clouds and this is due to their large opacity compared to the "clear" atmosphere. Even in presence of substantial aerosol and cirrus layers, the clear atmosphere is easily penetrated by the laser beam. On-beam lidar returns from a dense cloud of course enable its detection and ranging (cielometry from below, cloud-top height from an airborne platform) and, with some effort, information about the water phase can also be inferred (Platt et al., 1994). NASA's 1994 Lidar In space Technology Experiment or "LITE" (Winker et al., 1996), changed this situation radically. Indeed, pulses returned from marine stratocumulus (Sc) to the shuttle-based lidar system in a 260 km orbit were significantly stretched, to the point were they appear to originate from below sea-level! It was soon realized that this was not an instrumental artifact but a direct consequence of multiple scattering (Winker, 1996). Multiply-scattered radiance dominates the LITE signal because of the orbital geometry: the beam's width at cloud-level was about 300 m and the (night-time) detector's foot-print was over 900 m. So all orders-of-scattering (up to 1000's) contribute. How to determine cloud properties from LITE-type data is currently being researched (Miller and Stephens, 1998); specific ideas are proposed here. Because of the critical importance of multiple scattering in its cloud observations, we consider LITE as a forerunner of "off-beam" lidar.

We define off-beam lidar as any utilization of the portion of the lidar return *not* modeled by the lidar equation *nor* the modifications thereof for multiple scatterings in the forward direction (Flesia and Schwendimann, 1995) before and/or after the "main event," the quasi-backscatter. In other words, we are interested in the paths of photons that suffered at least one side-scatter.

In this paper we present the theory of off-beam cloud lidar from the standpoint of Green functions (GFs) for radiative transfer. From this perspective (section 2), off-beam lidar is a straightforward generalization of passive solar-spectrum remote sensing of clouds in the sense that it exploits the strong time-dependence and/or localization of the photon source, the Sun being a steady and uniform source. This naturally gives access to more physical cloud properties than optical depth (and effective droplet radius if a second spectral channel is used). By making an assumption about the radiation transport —photon diffusion dominates— and another about the cloud's structure —it is homogeneous— GF theory becomes tractable. We derive analytical results (section 3), apply them to cloud remote sensing (section 4), extend their validity numerically to realistic cloud models (section 5) and empirically to real-world clouds (section 6), and conclude with remarks on the practical problems of off-beam signal detection (section 7).

Correspondence to: Anthony B. Davis (adavis@lanl.gov)

GF theory informs us that both physical and optical cloud thicknesses can be retrieved from the data. While optical thickness is routinely retrieved by passive solar and microwave remote-sensing, mm-radar is the only other remote-sensing technique for obtaining physical thickness; also quite new, its definition of cloud boundary often does not agree with standard cielometry (Clothiaux et al., 1995).

2 Green Function (GF) Theory Applied to Lidar

2.1 Definitions for Plane-Parallel Cloud Geometry

2.1.1 GF for a Boundary Source

Let $t > 0$ denote the time when and $\boldsymbol{r} = (x,y,z)^{\mathrm{T}} \in \Re^3$ the position where we measure the flux of photons flowing in direction $\Omega = (\Omega_x,\Omega_y,\Omega_z)^{\mathrm{T}}$, a unit 3-vector. (Superscript "T" means transpose.) This time-dependent radiation field results from a pulse of photons released instantaneously at $t^* = 0$, in the direction $\Omega^* = (\Omega^*_x,\Omega^*_y,\Omega^*_z)^{\mathrm{T}}$, from $\boldsymbol{r}^* = \boldsymbol{0}$ which is assumed to be on one of the cloud's horizontal boundaries ($z = 0$, $z = \Delta_z$). The z-axis is vertical, oriented either up or down, in such a way that $\Omega^*_z > 0$.

Mathematically, we seek $G(t,\boldsymbol{r},\Omega;t^*,\boldsymbol{r}^*,\Omega^*)$ as solution of the non-stationary radiative transfer equation:

$$[\, c^{-1}\partial_t + \Omega\bullet\nabla \,]\, G = -\sigma_{\mathrm{tot}}(\boldsymbol{r})G + \sigma_{\mathrm{sca}}(\boldsymbol{r}) \int p(\Omega'\to\Omega)\, G(t,\boldsymbol{r},\Omega';\cdot)\, \mathrm{d}\Omega', \tag{1}$$

with boundary/initial conditions

$$\begin{aligned} &G(t,\boldsymbol{r},\Omega;\cdot) = \delta(t)\delta(x)\delta(y)\delta(\Omega-\Omega^*), && t>0,\ z=0, && \Omega_z>0,\\ &G(t,\boldsymbol{r},\Omega;\cdot) = 0, && t>0,\ z=\Delta_z, && \Omega_z<0,\\ &G(t,\boldsymbol{r},\Omega;\cdot) = 0, && t=0,\ 0<z<\Delta_z, && \forall\Omega, \end{aligned}$$

where $\boldsymbol{x} = (x,y)^{\mathrm{T}} \in \Re^2$. (2)

Note that the cloud is assumed (geometrically) plane-parallel but not homogeneous (yet): $\sigma_{\mathrm{tot}}(\boldsymbol{r})$ and $\sigma_{\mathrm{sca}}(\boldsymbol{r})$ are the possibly $\boldsymbol{r}$-dependent total and scattering extinction coefficients, respectively; $p(\Omega'\to\Omega)$ is the scattering phase function that we assume depends only on scattering angle $\theta_s = \cos^{-1}(\Omega'\bullet\Omega)$.

$G(t,\boldsymbol{r},\Omega;t^*,\boldsymbol{r}^*,\Omega^*)$ is the Green function (GF) for linear transport in a plane-parallel medium with boundary sources. Kornreich and Ganapol (1997) analytically computed the GF in the limit $\Delta_z \to \infty$ without time-dependence for isotropic scattering ($p(\theta_s) \equiv 1/4\pi$) by reducing it to Chandrasekhar H-functions via (x,y)-Fourier and z-Laplace transforms. Further on, we will see that the problem posed in Eqs. (1–2) must be considerably simplified to make analytical progress with more realistic cloud geometry and optical properties.

The main utility of the GF is that it can be used to obtain the radiation field for arbitrary illumination conditions (at a boundary in this case) by direct summation of its space-time translates, i.e., convolution with a space-time source distribution. Marshak et al. (1998) use this linear convolution property to model nonlinear 3D radiative transfer effects on boundary fluxes (activation of horizontal fluxes by fluctuations of the optical density field) and apply their results to cloud remote sensing in the solar spectrum.

Similarly, we can sum over sources in direction-space. For instance,

$$G_{\mathrm{iso}}(t,\boldsymbol{r},\Omega;t^*,\boldsymbol{r}^*) = \int_{\Omega^*_z>0} \Omega^*_z G(t,\boldsymbol{r},\Omega;t^*,\boldsymbol{r}^*,\Omega^*)\, \mathrm{d}\Omega^* \tag{3}$$

is the temporal-spatial-angular response (used extensively further on) to a directionally isotropic burst of photons emanating from a single boundary point.

In the following, we consider the Dirac δ-source in Eq. (2) simply as a convenient mathematical model for a pulsed laser beam emitted from a lidar. The GF thus models the cloud's response to the laser source; accordingly, we take

$$\Omega^* = \hat{z} = (0,0,1)^{\mathrm{T}} \tag{4}$$

since we consider zenith-pointing systems.

2.1.2 Remotely Observable GFs

We are primarily interested in the part of the GF that can be observed remotely; this restricts us to $z \le 0$ with $\Omega_z \le 0$ (reflection) or $z \ge \Delta_z$ with $\Omega_z \le 0$ (transmission). With lidar applications in mind, we will concentrate on monostatic configurations: the source and the detector are collocated at a distance δ_{obs} from the cloud ($-\infty < z_{\mathrm{obs}} = -\delta_{\mathrm{obs}} < 0$). This leads to a function $G_{\mathrm{obs}}(t,\Omega(x,y);t^*,x^*,y^*)$ where (x,y) are the horizontal coordinates of the intercept of the (illuminated) boundary plane $z = 0$ with the ray of light arriving at $\boldsymbol{r}_{\mathrm{obs}} = (x^*,y^*,-\delta_{\mathrm{obs}})$ from direction Ω. Figure 1 illustrates two situations of practical interest: δ_{obs} is a few times Δ_z (ground-based observation) and $\delta_{\mathrm{obs}} \gg \Delta_z$ (satellite-based observation). Davis et al. (1998) report on the first laboratory measurements of $G_{\mathrm{obs}}(t,\Omega(x,y);t^*,x^*,y^*)$.

Without loss of generality, we can set $t^* = 0$ and, apart from a trivial increment in time involving δ_{obs} and the slant viewing geometry, the remotely observable GF is equal to $G(t,x,y,0,\Omega(x,y);0,x^*,y^*,0,\hat{z})$ in absence of extinction in the intervening region $-\delta_{\mathrm{obs}} < z < 0$. In contrast, we can not express this as a function of (x^*-x,y^*-y) as is customary in text-book GF theory because the extinction coefficients in Eq. (1) generally depend on the horizontal coordinates.

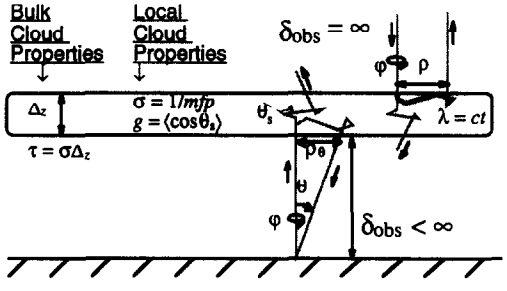

Fig. 1. *Schematic of off-beam lidar observations from ground and space.*

It is probably not feasible in practice to sample the remotely observable GF, $G_{obs}(t,\Omega(x,y);x^*,y^*)$, continuously in angle-space. Figure 2 shows a discretely-sampled spatial GF obtained in a numerical experiment using an internally homogeneous cloud at range δ_{obs} = 1 km with: a realistic "C1" phase function; physical thickness Δ_z = 0.3 km; and optical depth $\tau = \sigma\Delta_z$ = 13 (all typical of a marine Sc layer).

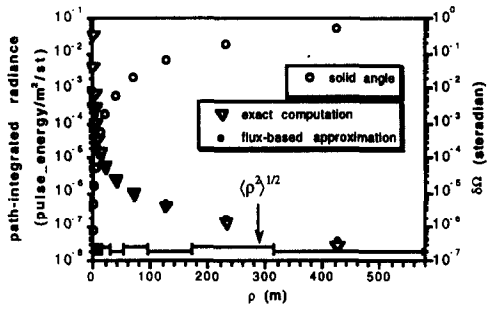

Fig. 2. *Discretized Observable GF.* To keep time-integrated flux roughly constant in the various angular bins, their size increases exponentially (cf. solid angles on r.h. axis) with radial distance from the optical axis; see Davis and Cahalan (1998) for details. Bin-averaged radiance (l.h. axis) is computed in two ways: an exact sum of local estimates in a forward Monte Carlo run with 10^7 histories, and an isotropic (Lambertian) redistribution of surface flux for the area subtended by the solid-angle bin.

2.1.3 GFs for Photon Escape

Although this is not practical to do outside of a laboratory, it is of interest to measure as best we can the time-dependent flux field at the cloud boundaries. Namely,

$$G_R(t,x,y;x^*,y^*) = \int_{\Omega_z<0} |\Omega'_z| G(t,x,y,0,\Omega;x^*,y^*)\, d\Omega \qquad (5a)$$

in reflection, and similarly in transmission,

$$G_T(t,x,y;x^*,y^*) = \int_{\Omega_z>0} \Omega_z G(t,x,y,\Delta_z,\Omega;x^*,y^*)\, d\Omega \qquad (5b)$$

In absence of detailed information about the (space/time-dependent) bi-directional properties of the cloud's GFs, we make a standard Lambertian hypotheses:

$$G(t,x,y,0,\Omega;x^*,y^*) \equiv G_R(t,x,y;x^*,y^*) / \pi, \qquad (6a)$$
$$G(t,x,y,\Delta_z,\Omega;x^*,y^*) \equiv G_T(t,x,y;x^*,y^*) / \pi. \qquad (6b)$$

This assumption proves reasonable in the case of dense clouds (cf. Fig. 2) and $G_R(t,x,y;x^*,y^*)$ can thus be estimated from a remote measurement of $G_{obs}(t,\Omega(x,y);x^*,y^*)$, as introduced in sub-section 2.1.2; equivalently (in absence of out-of-cloud extinction), we have $G(t,x,y,0,\Omega(x,y);x^*,y^*)$ in Eq. (6a). More sophisticated radiance-to-flux conversions, akin to those used in satellite-based radiation budget studies, could be used if necessary.

2.1.4 Azimuthally-, Spatially- and Ensemble-Averaged GFs

As already mentioned, boundary-source GFs for a cloud with nontrivial horizontal structure will depend on both (x,y) and (x^*,y^*), not only their difference. This "2+1" dimensional dataset for every choice of (x^*,y^*), would be at best difficult to use for cloud remote sensing. However, in a field experiment we can average the GF azimuthally (assuming statistical isotropy) and/or spatially (assuming statistical homogeneity, sometimes called stationarity). In a numerical or analytical exercise using randomly variable cloud models, we can average over the "disorder." Such ensemble-averaged GFs are reasonable surrogates for their observed counterparts (under an "ergodicity" assumption).

We will deal here with either homogeneous clouds or average GFs. In the remainder, we therefore drop from the GF's arguments all those describing the source.

2.2 GFs as a Unified Framework for Cloud Remote Sensing, Passive and Active

2.2.1 Probabilistic Interpretation of GFs

Photon-escape GFs have straightforward interpretations in terms of probability of a photon to escape from the cloud (into any direction) at position $\boldsymbol{x} = (x,y)^T$ and time t, conditional to be either reflected or transmitted: e.g.,

$$G_R(t,x,y)dxdydt / R = \text{Prob}\{\text{ escape during } [t,t+dt), \text{ from } [x,x+dx)\otimes[y,y+dy) \mid \text{ in reflection } (z=0, \Omega_z<0)\ \}, \qquad (7)$$

where the normalization constant,

$$R = \iiint G_R(t,x,y)dxdydt, \qquad (8)$$

is simply the cloud's albedo for normal incidence. Similar relations can be written for the event of transmission where, by conservation, $T = 1-R$. Normalized escape GFs can thus be treated as probability density functions (PDFs) and we can compute their moments.

2.2.2 Low-Order Statistical Moments of GFs

The simplest characteristics of a laser pulse's propagation in a cloud are: mean photon pathlength (denoted $\lambda = ct$),

$$\langle\lambda\rangle_R = c\langle t\rangle_R = c\iint dxdy\left[\int t G_R(t,x,y)dt\right] / R; \qquad (9a)$$

its 2nd-order moment (used in path variance $\langle\lambda^2\rangle_R - \langle\lambda\rangle_R{}^2$),

$$\langle\lambda^2\rangle_R = c^2\langle t^2\rangle_R = c\iint dxdy\left[\int t^2 G_R(t,x,y)dt\right] / R; \qquad (9b)$$

root-mean-square (rms) horizontal transport $\sqrt{\langle\rho^2\rangle_R}$, where

$$\langle\rho^2\rangle_R = \int dt\left[\iint (x^2+y^2)G_R(t,x,y)dxdy\right] / R \qquad (10)$$

since $\langle x\rangle_R = \langle y\rangle_R = 0$ by symmetry. Similar quantities are defined for transmission.

The quantities in Eqs. (9a,b) can be measured directly form LITE data, using the radiance-to-flux conversion in Eq. (6a) or simply redefining the mean pathlength using radiance in lieu of flux. It can also be obtained indirectly, using oxygen A-band spectroradiometry at sufficiently high resolution and the "equivalence" theorem (van de Hulst, 1980; Stephens and Heidinger, 1998). In the latter approach, the photon source is the Sun and the instrument is either below or above the atmosphere. Pfeilsticker et al. (1998) report on the first successful measurements from ground of $\langle\lambda\rangle_T$ and the second moment $\langle\lambda^2\rangle_T$.

To date, the quantity in Eq. (10) has not been measured directly. It has been estimated indirectly using the small-scale properties of high-resolution LANDSAT cloud scenes (30-m pixels). Specifically, Davis et al. (1997b) used numerical simulations to show that the LANDSAT "scale-break" is a manifestation of 3D radiative transfer. [This scale-break is a well-documented deficit in the variability of nadir radiance at small scales with respect to the known variability of the clouds' liquid water content.] This statistical phenomenon occurs at 200–300 m and is traceable to a radiative "smoothing" (Marshak et al., 1995) that affects scales smaller than a few $\langle\rho^2\rangle_R^{1/2}$.

2.2.3 Significance of the GF's Fourier-Laplace Expansion

Define the Fourier-Laplace transform of the *R*-escape GF:

$$\tilde{G}_R(s,k_x,k_y) = \iiint \exp[-st+i(k_x x+k_y y)]G_R(t,x,y)\mathrm{d}t\mathrm{d}x\mathrm{d}y; \quad (11)$$

and similarly for transmission. We now expand this function in a multidimensional Taylor series:

$$\begin{aligned}\tilde{G}_R(s,k_x,k_y) = \tilde{G}_R(s,\boldsymbol{k}) = \tilde{G}_R(0,\mathbf{0}) \\ + s[\partial_s \tilde{G}_R](0,\mathbf{0}) \\ + \boldsymbol{k}\bullet[\nabla_{\boldsymbol{k}}\tilde{G}_R](0,\mathbf{0}) \\ + \tfrac{1}{2}s^2[\partial_s^2\tilde{G}_R](0,\mathbf{0}) \\ + \tfrac{1}{2}[\boldsymbol{kk}]:[\nabla_{\boldsymbol{k}}\nabla_{\boldsymbol{k}}\tilde{G}_R](0,\mathbf{0}) \\ + \textit{crossed and higher-order terms}\end{aligned} \quad (12)$$

where ":" means a double contraction on the dyadic tensors.

Interestingly, each coefficient in this expansion in s and $\boldsymbol{k}$ has a specific meaning in cloud remote sensing:

- $\tilde{G}_R(0,\mathbf{0}) = R$ (13a)
  in Eq. (8), i.e., passive solar-spectrum approaches;
- $[\partial_s^q\tilde{G}_R](0,\mathbf{0}) = \langle t^q\rangle_R = \langle\lambda^q\rangle_R/c^q$ $(q = 1,2)$, (13b)
  in Eqs. (9a,b), i.e., LITE or A-band (from above);
- $\mathrm{Tr}[\nabla_{\boldsymbol{k}}\nabla_{\boldsymbol{k}}\tilde{G}_R](0,\mathbf{0}) = \langle\rho^2\rangle_R$ (13c)
  in Eq. (10), no direct observations yet (out of the lab).

The 1st-order $\boldsymbol{k}$-gradients in (12) and associated moments $(\langle x\rangle_R,\langle y\rangle_R)$ vanish by symmetry, as do off-diagonal terms in the 2nd-order tensor (associated with $\langle xy\rangle_R = \langle yx\rangle_R = 0$).

We now show that $\tilde{G}_R(s,\boldsymbol{k})$ can be computed analytically under certain conditions. This means that the measurable quantities in Eqs. (8–10) can be expressed as closed-form functions of optical and structural cloud parameters.

3 Analytical GF Theory

3.1 The Diffusion Approximation in 3D Radiative Transfer

Radiative transfer in clouds —at least dense boundary-layer stratus and cumulus— is dominated by multiple scattering. There is compelling evidence uncovered by King et al. (1990), using *in situ* radiometry, for the existence of an extensive "diffusion domain" for solar photon transport inside marine Sc. From the modeling perspective, this means asymptotic (large optical depth) theory can be invoked for radiance (van de Hulst, 1980), photon diffusion for flux. We will put ourselves in the latter framework, equivalent to an Eddington approximation in 3D.

A key quantity in diffusion theory is "scalar" flux:

$$J(t,\boldsymbol{r}) = \int G(t,\boldsymbol{r},\Omega)\,\mathrm{d}\Omega, \quad (14a)$$

a.k.a. $4\pi \times$ *mean_radiance* or $c \times$ *radiant_energy_density*; the other important quantity is radiant energy flux vector:

$$\boldsymbol{F}(t,\boldsymbol{r}) = \int \Omega G(t,\boldsymbol{r},\Omega)\,\mathrm{d}\Omega. \quad (14b)$$

Equations (14a,b) are actually the two first terms in a full spherical-harmonic expansion of the angular distribution of radiance at $(t,\boldsymbol{r})$. A similarly truncated expansion is required for the differential cross-section (per unit of path) for scattering, namely, $\sigma_{sca}(\boldsymbol{r})p(\Omega'\cdot\Omega)$:

$$\sigma_{sca}(\boldsymbol{r})\int p(\Omega'\cdot\Omega)\mathrm{d}\Omega = \sigma_{tot}(\boldsymbol{r})\varpi_0, \quad (15a)$$

where $\varpi_0 = \sigma_{sca}(\boldsymbol{r})/\sigma_{tot}(\boldsymbol{r})$ is the single-scattering albedo, the integral of $p(\Omega'\cdot\Omega)$ being normalized to unity; and

$$\sigma_{sca}(\boldsymbol{r})\int \Omega'\cdot\Omega p(\Omega'\cdot\Omega)\mathrm{d}\Omega = \sigma_{tot}(\boldsymbol{r})\frac{\varpi_1}{3} = \sigma_{tot}(\boldsymbol{r})\varpi_0 g \quad (15b)$$

where $g = \varpi_1/3\varpi_0$ is the asymmetry factor.

$J(t,\boldsymbol{r})$ and $\boldsymbol{F}(t,\boldsymbol{r})$ obey two independent constraints. First, they enter the (exact) law of radiant energy conservation,

$$c^{-1}\partial_t J + \nabla\bullet\boldsymbol{F} = -\sigma_{tot}(\boldsymbol{r})(1-\varpi_0)J, \quad (16)$$

which follows from Eq. (1) and the definitions in Eqs. (14a,b) and (15a). Second, they are related by Fick's law for photon diffusion, operating as a constitutive relation that "closes" the transport problem in Eq. (16),

$$\boldsymbol{F}(t,\boldsymbol{r}) = -\frac{1}{3}\ell_t(\boldsymbol{r})\nabla J, \quad (17)$$

where $\ell_t(\boldsymbol{r})$ is the "transport" mean-free-path (mfp):

$$\ell_t(\boldsymbol{r}) = [(1-\varpi_0 g)\sigma_{tot}(\boldsymbol{r})]^{-1}. \quad (18)$$

In essence, ℓ_t is the "effective" mfp for isotropic scattering in the sense following sense. After a single step, the photon propagates $1/\sigma_{tot}$ on average, then undergoes a scattering; after a large number of forward-peaked Mie scatterings, the photon has propagated $(1-\varpi_0 g)^{-1}$ times further, and all but "forgotten" its original direction of propagation.

3.2 Diffusive GFs for Homogeneous Plane-Parallel Clouds

In the remainder, we consider pure scattering ($\varpi_0 = 1$) which means a choice of laser wavelength where there is no absorption by droplets or interstitial gases. Whenever necessary, we will set $g \approx 0.85$, the canonical value for cloud droplet populations; this yields $(1-g)^{-1} \approx 6.7$.

For r-independent extinction coefficients, Eqs. (16–17) can then be combined into the standard parabolic PDE:

$$\partial_t J = D\nabla^2 J, \tag{19}$$

with constant radiative "diffusivity"

$$D = c\ell_t/3 = c/[3(1-g)\sigma]. \tag{20}$$

Following standard procedure in mathematical physics, this PDE can be (horizontal) Fourier- and (time) Laplace-transformed into an ODE where z is the only independent variable. The resulting ODE is formally equivalent to that of the homogeneous/steady-state 2-stream problem in 1D with a radiant energy sink (absorption-like) term,

$$\tilde{J}'' - \tilde{J}/L^2 = 0, \tag{21}$$

where the coefficient of the pseudo-sink term contains the Fourier-Laplace conjugate variables $k = \|\mathbf{k}\|$ and s:

$$1/L^2 = k^2 + s/D. \tag{22}$$

After angular integration, the collimated boundary source is indistinguishable from an isotropic one, so we are actually computing the GF in Eq. (3). The boundary/initial conditions in Eq. (2) are Fourier-Laplace transformed into the following ones for the ODE in Eq. (21):

$$\tfrac{1}{2}\,[1 - (\chi\ell_t)\tfrac{d}{dz}]\tilde{J} = 1, \text{ at } z = 0, \tag{23a}$$

$$\tfrac{1}{2}\,[1 + (\chi\ell_t)\tfrac{d}{dz}]\tilde{J} = 0, \text{ at } z = \Delta_z, \tag{23b}$$

where $\chi\ell_t$ is the extrapolation length (Case and Zweifel, 1967). An $O(1)$ numerical constant weakly dependent on τ, χ is essentially a free parameter determined by matching diffusion-based results to detailed numerical computations.

Equations (21) and (23) define a 2-point boundary value problem for $\tilde{J}$ that is easily solved although the expression for $\tilde{J}(s,k,z)$ is quite involved. It depends on z and $L(s,k)$, that includes $D(g,\sigma)/c = \ell_t(g,\sigma)/3$, and two other constant length scales: $\chi\ell_t(g,\sigma)$, and Δ_z. Explicitly, we have

$$\tilde{J}(L(s,k),z) = 2\times\frac{(1+\chi\ell_t/L)e^{(\Delta_z-z)/L} - (1-\chi\ell_t/L)e^{-(\Delta_z-z)/L}}{(1+\chi\ell_t/L)^2 e^{\Delta_z/L} - (1-\chi\ell_t/L)^2 e^{-\Delta_z/L}}. \tag{24}$$

Fourier-Laplace transforms of the surface flux-fields in Eq. (5) are the formal counterparts of reflectance and transmittance in the associated 2-stream problem, hence (Case and Zweifel, 1967):

$$\tilde{G}_R(s,k) = \tfrac{1}{2}\,[1 + \chi\ell_t\tfrac{d}{dz}]\tilde{J}|_{z=0} = \tilde{J}(s,k,0) - 1, \tag{25a}$$

$$\tilde{G}_T(s,k) = \tfrac{1}{2}\,[1 - \chi\ell_t\tfrac{d}{dz}]\tilde{J}|_{z=\Delta_z} = \tilde{J}(s,k,\Delta_z). \tag{25b}$$

Substituting Eq. (24) into these leads respectively to:

$$\tilde{G}_R(L(s,k)) = \frac{1-(\chi\ell_t/L)^2}{1 + 2(\chi\ell_t/L)\coth(\Delta_z/L) + (\chi\ell_t/L)^2}, \tag{26a}$$

$$\tilde{G}_T(L(s,k)) = \frac{2(\chi\ell_t/L)\operatorname{cosech}(\Delta_z/L)}{1 + 2(\chi\ell_t/L)\coth(\Delta_z/L) + (\chi\ell_t/L)^2}. \tag{26b}$$

3.3 Expressions for Low-Order Moments of Reflected GFs

Unfortunately, the above expressions can not be inverse-transformed back into physical (t,x,y)-space. This prevents us from having analytic PDFs for the photon escape events but we can still compute their moments. Indeed, since an analytic expression exists for $\tilde{G}_R(s,k)$ in Eqs. (11–12) its low-order Taylor coefficients in Eq. (13) can be computed explicitly in terms of cloud parameters.

Equivalently, we need a 4th-order (3-term) expansion in $1/L$ of the (L-symmetric) expression (26a) to reach the 2nd-order moment in time in Eqs. (12–13). It is convenient to use here a unit of length where $\ell_t = 1$, meaning that χ is now the extrapolation length itself and that Δ_z is now the rescaled optical depth $(1-g)\tau$. Some algebra then leads to:

$$\begin{aligned}\tilde{G}_R(s,k) = \frac{\Delta_z}{\Delta_z+2\chi}\times[\,1 \\ - \frac{2\chi}{\Delta_z+2\chi}\times(\tfrac{1}{3}\Delta_z{}^2+\chi\Delta_z+\chi^2)\,/\,L^2 \\ + \frac{2\chi\Delta_z}{(\Delta_z+2\chi)^2}\times(\tfrac{1}{45}\Delta_z{}^4+\tfrac{4}{15}\chi\Delta_z{}^3+\chi^2\Delta_z{}^2+\tfrac{5}{3}\chi^3\Delta_z+\chi^4)\,/L^4 \\ +\ \textit{higher-order terms}\ ]\end{aligned} \tag{27}$$

Davis and Marshak (1996) did a similar computation to order 2 in a 2D setting, where "3" becomes "2" in Eq. (20) for diffusivity D which, in turn, enters only via the Jacobian

$$\frac{\partial}{\partial s}L^{-2} = \frac{1}{D} = \frac{d}{\ell_t c}\,(d = 1,2,3) \tag{28}$$

required to compute temporal statistics; dimensionality d also affects trivially the horizontal transport term in Eq. (13c): the number of identical diagonal elements is d–1.

Returning to the nondimensional definition of χ, we find:

$$R = \frac{\Delta_z}{\Delta_z+2\chi\ell_t} = \frac{(1-g)\tau}{(1-g)\tau+2\chi\ell_t} \tag{29a}$$

for albedo;

$$\langle\lambda\rangle_R = \frac{2d\chi}{3}\times\Delta_z\times[\,1 + C_R(\frac{\chi}{(1-g)\tau})\,] \tag{29b}$$

for mean pathlength in $d = 1$, 2, or 3 dimensions; and

$$\langle\rho^2\rangle_R = (d-1)\times\frac{4\chi}{3}\times\frac{\Delta_z{}^2}{(1-g)\tau}\times[\,1 + C_R(\frac{\chi}{(1-g)\tau})\,] \tag{29c}$$

for variance in horizontal transport. The two latter quantities contain a pre-asymptotic correction term:

$$C_R(\varepsilon) = \varepsilon(1+3\varepsilon)/(1+2\varepsilon); \tag{30}$$

this correction becomes small as $(1-g)\tau/\chi = 1/\varepsilon$ increases. We note that, apart from proportionality constants, leading terms in (29b,c) can be obtained from simpler arguments based on the fractal properties of photon random walks in the finite slab that defines the cloud (Davis et al., 1997a).

The angular integration of the boundary/initial conditions in Eq. (2) has, in effect, forced us to use the "iso" fields defined as in Eq. (3). The 2-stream problem at the core of the above 1D computations can be recast for a collimated beam in 3D by reformulating Eq. (1) with an internal source term and accordingly homogeneous boundary- and initial-conditions in Eq. (2). This will lead to more accurate but also more complex expressions. We do not anticipate any qualitative difference in the leading terms, only in the (non-negligible) correction terms.

4 Applications to Cloud Remote Sensing

Returning to Eqs. (13a–c), the obvious remote-sensing interpretations of Eqs. (29a–c) are:

29a: single-wavelength passive approach with no access to physical thickness Δ_z, only to τ (for known g);

29b: pulse-shapes returned to LITE were primarily dependent on Δ_z (with τ-dependent corrections);

29a,b: calibrated active approaches (including LITE data), can be used to determine Δ_z and τ simultaneously;

29b,c: un-calibrated active approach with imaging (or at least radial profiling) capability can yield Δ_z and τ.

Figure 3a conventionally illustrates this last technique: a curvilinear array of lines of constant Δ_z and τ plotted versus two observables: $\langle\lambda\rangle_R$ and $\langle\rho^2\rangle_R^{1/2}/\langle\lambda\rangle_R$. This choice of independent variables yields iso-parameter lines orthogonal enough to separate τ and Δ_z, at least in the domain where diffusion theory is accurate in its current status: $(1-g)\tau > 1$. This bound can be lowered substantially by relaxing the isotropic source assumption implicit in Eqs. (21–23).

An alternate approach to (Δ_z,τ)-retrieval requiring neither absolute calibration nor imaging capability uses mean and variance of the pathlength distribution. Indeed, using the corresponding terms in Eq. (27), it can be shown that the lowest-order moments are independent functions of (Δ_z,τ):

$$\langle\lambda\rangle_R \approx 2\chi\Delta_z, \text{ and } \langle\lambda^2\rangle_R \approx \frac{4\chi}{5}\Delta_z^2(1-g)\tau \tag{31}$$

in $d = 3$ (leading terms only, after restoring χ to $\chi\ell_t$). So τ can in principle be inferred from

$$\langle\lambda^2\rangle_R/\langle\lambda\rangle_R^2 \approx (1-g)\tau/5\chi. \tag{32}$$

For this technique to work, τ needs to be large enough (and/or ℓ_t small enough) that $\Delta_z^4/45 > (4/15)\chi\ell_t\Delta_z^3$ in Eq. (27), hence $\Delta_z/\chi\ell_t = (1-g)\tau/\chi > 12$, where $\chi = 0.7104\cdots$ for large $(1-g)\tau$ (Case and Zweifel, 1967) and $g = 0.85$; in summary, $\tau > 56$ —an extreme value for most cloud types. With the correction term (30) and a more complicated one for the 2nd-order moment, this bound on τ can be lowered to $(1-g)\tau/\chi > 1.596\cdots$. Below this value, the analytical model gives rise to negative λ-variances as diffusion theory loses its accuracy, when Δ_z/ℓ_t becomes $O(1)$ and less: boundary effects (extending over a distance $\approx\ell_t$) are poorly treated. In the limit of optically thin media in $d = 3$ we have $\chi = 4/3^-$ (Case and Zweifel, 1967), leading to $\tau > 14$. Numerically generated look-up tables are required for lower values of τ. Figure 3b illustrates the general idea.

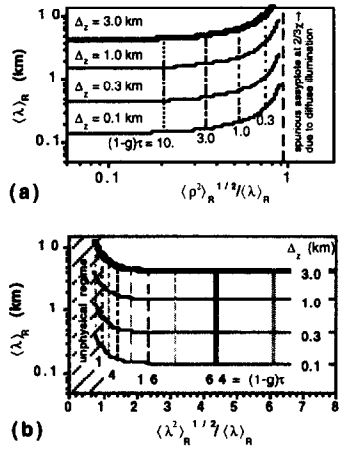

Fig. 3. *Two techniques for remote-sensing of cloud parameters Δ_z and τ, given g, without calibration.* **(a)** Space-time scheme uses mean pathlength and rms spot-size (requires imaging capability). **(b)** Time-only (LITE-type) scheme using 1st and 2nd moments of the returned pulse shape.

5 Numerical Validation and Extension of GF Theory

To validate diffusive GF theory, we solve the nonstationary transfer problem in Eqs. (1–2) with Monte Carlo methods.

5.1 Homogeneous cloud models

Figure 4 compares numerical estimates of the low-order spatial- and temporal moments in Eqs. (9a), (9b) and (10) for

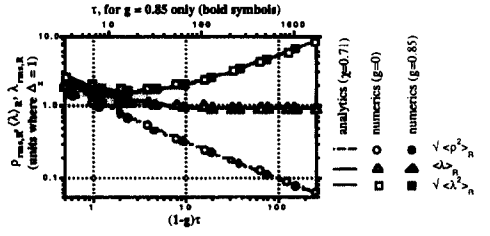

Fig. 4. *Numerical validation of analytical GF theory in* 2D ($d = 2$). Space- and time-statistics are plotted versus rescaled optical depth $(1-g)\tau$ in units of thickness Δ_z. Monte Carlo computations for a diffuse boundary point-source are in close agreement with predictions in Eqs. (27), (29b,c) and (30) for homogeneous plane-parallel clouds if τ is large enough.

homogeneous clouds in $d = 2$ with analytical predictions from Eqs. (13) and (27). Both isotropic scattering and a 2D counterpart of the Heney-Greenstein phase-function:

$$p(\theta_s) = \frac{d}{d\theta_s} \text{Prob}\{\theta \to \theta + \theta_s\} = \left(\frac{1}{2\pi}\right) \frac{1-g^2}{1+g^2-2g\cos\theta_s} \quad (33)$$

with $g = 0.85$, were used. Cloud thickness Δ_z was held constant while optical depth τ was varied from 0.5 to 256 for $g = 0$, 1024 for $g = 0.85$. Photon source was point-wise but isotropic to promote diffusion as close as possible to the boundary. Agreement is excellent for $(1-g)\tau > 2$.

Figures 5a,b show results for mean pathlength and rms spot-size for homogeneous clouds in $d = 3$. Illumination here is collimated, normal to the boundary and scattering is modeled with a standard Heney-Greenstein phase-function:

$$p(\theta_s) = \frac{d}{d\Omega} \text{Prob}\{\Omega \to \Omega'\} = \left(\frac{1}{4\pi}\right) \frac{1-g^2}{(1+g^2-2g\cos\theta_s)^{3/2}} \quad (34)$$

for $g = 0.0$ and 0.85. Agreement is still good, especially for spot-size in panel (b), in the asymptotic limit (large τ). At least for mean pathlength in panel (a), the pre-asymptotic results fail to collapse onto a universal function of $(1-g)\tau$; a refined diffusion theory can possibly account for this.

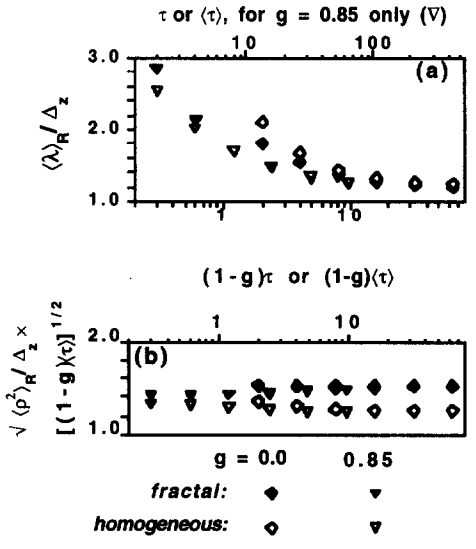

Fig. 5. *Numerical generalization of analytical GF theory in* 3D ($d = 3$). Monte Carlo computations (by Dr. Alexander Marshak) for a pulse of photons in a collimated beam impinging on homogeneous and fractal cloud models, as illustrated in Fig. 4. **(a)** Mean pathlength in Eqs. (9a) and (29b). **(b)** Root-mean-square spot-size from Eqs. (10) and (29c).

5.2 Fractal cloud models

To extend our key results (29b,c) to more realistic cloud models, we used "bounded cascades" to redistribute cloud liquid water inside an otherwise plane-parallel cloud; we thus simulate an extended stratus layer. The resulting PDF for optical depth is strongly skewed towards larger τ's (Cahalan, 1994) and its 2-point correlations are multifractal (Marshak et al., 1994); both properties are required to match those of real clouds (Ivanova and Ackerman, 1998). A few realizations were used and the GF was further averaged over space, as described in sub-section 2.1.4.

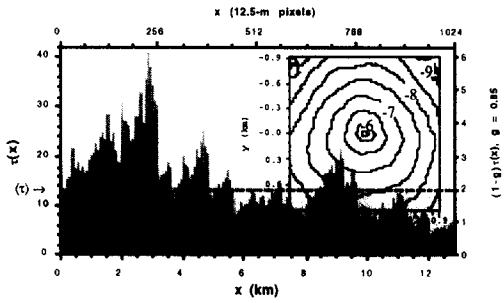

Fig. 6. *Typical multifractal model for optical depth variability.* The cloud is still geometrically plane-parallel but extinction varies horizontally. Inset: GF for escape from a 3D cloud (isophotes at logarithmic intervals).

Variability in optical depth τ can unfold in the x-direction only (as exemplified by 1D τ-field in Fig. 6) or in 2D (as exemplified by the GF inset in Fig. 6). The observed scaling range of 3 decades is more easily reached in 1D: 12.8-km domain, 1024-pixels, 12.5-m pixels (for 300 m thickness). However, conclusions are not changed by using a 2D grid to model the variability. Figures 5a,b show Monte Carlo results as a function of mean optical depth $\langle\tau\rangle$:

- Fractal structure has little effect on the mean pathlength in panel (a); this is clearly related to the fact that the variable quantity, τ, appears only in the correction term in Eq. (29b). We anticipate stronger variability effects in the pathlength's variance, skewness, etc.
- Fractal structure only affects the proportionality constant in Eq. (29c), making larger rms-ρ's in panel (b). This shift is consistent with Jensen's inequality[1] if one averages the r.h. side of Eq. (29c) over the variability in τ, ignoring the correction term in Eq. (30).

The natural resolution of an off-beam lidar system is roughly 2–3 times $\langle\rho^2\rangle_R^{1/2}$ from Eq. (29c) or Fig. 5b, which is expected to be ≈0.5 km for marine Sc ($\langle\tau\rangle = 13$, $\Delta_z = 0.3$ km), somewhat more in continental boundary-layer clouds. There is enough horizontal variability on scales smaller than this to affect the observables in Figs. 3a,b.

6 Empirical Results for Real Clouds in CW Mode

Measurement of off-beam lidar returns is a challenge, especially in day-time when there is fierce competition between laser and solar photons. Nevertheless, Davis et al. (1997c) used a relatively standard zenith-pointing research lidar system to see how far away from the vertical axis they

[1] For instance, $\langle R(\tau)\rangle \le R(\langle\tau\rangle)$ using Eq. (29a), cf. Cahalan (1994).

could track the off-beam signal. The Nd:YAG transmitter operated at 1.06 μm, delivering 15 W equivalent cw power. The detector, feed by a 40-cm Cassegrain telescope, had a quantum efficiency better than 50% and a narrow FOV (1.4 mrad); this last characteristic is typical in on-beam lidar but unnecessarily small for the present application.

The system was operated in time- and pulse-averaging mode while the laser beam was deflected away from zenith by an angle controlled by a pair of small mirrors. Optical reciprocity guarantees this is equivalent to leaving the beam at zenith and tilting the telescope, a more cumbersome operation. Data was collected for a few minutes on Sept. 12, 1996; the sky was completely overcast (ceiling at ≈1.5 km) with an under-layer of broken cumulus (at ≈1 km).

The raw (uncalibrated) photo-diode output data is plotted versus angle θ in Fig. 7; they are overlaid with numerical predictions of the t-integral of $G(t,x,y,0,\Omega(x,y))|_{x=\rho(\theta),y=0}$ by Davis and Marshak (1996) for two homogeneous Heney-Greenstein clouds at 1 km range, extrapolated to 1.5 km. The only requirement on the double-ordinate semi-log plot is that both ranges (normalized radiance and mV's) be 5 orders-of-magnitude. Agreement is remarkable, bearing in mind the complexity of the real cloud cover and the simplicity of the computational models.

The important feature of this instrumental achievement is that, before the off-beam signal was lost in solar noise, a regime of exponential decay was reached and reasonably well sampled. Even the rms horizontal transport distance $\langle\rho^2\rangle_R^{1/2}$ defined operationally in Eq. (10) was exceeded (see markers on upper axis in Fig. 7). This proves that the photons contributing to the data had penetrated deeply into the cloud's diffusion domain before escaping; very many scatterings are required to do this.

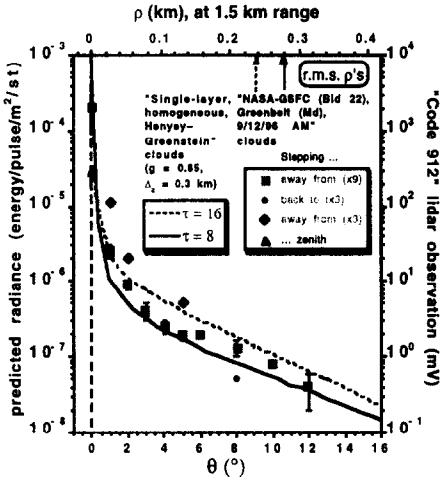

Fig. 7. *Off-beam lidar observations of a real cloud system in cw mode.* The data supports diffusive Green-function theory that predicts an exponential decay in the far-field: for large wave-number $k = 1/L$ in Eq. (26a), the Fourier transform of this field decays as a Lorentzian (in $1/k^2$).

7 Conclusion and Outlook

We described how off-beam lidar can be used to measure cloud thickness and density from ground, aircraft, or space. The two cornerstones of off-beam lidar theory are Green functions for the mathematics, and photon diffusion for the transport physics. Green function theory is analytically tractable for homogeneous plane-parallel cloud models and has been validated numerically. Monte Carlo simulations have also been used to extend the key theoretical results to more realistic cloud models with a fractal structure. Finally, path-integrated off-beam returns from real clouds were detected out to ≈0.3 km from the impact point of the laser beam on cloud base; these data follow the exponential trend predicted by diffusion theory. Both analytical and numerical modeling efforts needs refinement, including Rayleigh/aerosol scattering and in-cloud stratification.

The prospect of building sensitive and reliable off-beam lidar instruments is extremely good, at least for night-time operation. Photon-counting technology familiar to on-beam lidar can be used with adapted optics and detectors. The unusual requirement for off-beam lidar is to have imaging or, at least, radial profiling capability. One option is to use a holographic optical element (McGill et al., 1997); another is to use advanced low-light imaging/timing devices such as the one described by Preidhorsky et al. (1996). The main challenge is highlighted by Davis and Cahalan's (1998) signal-to-noise ratio (SNR) estimation: presence of an intense solar background; the authors list ways the *a priori* unfavorable SNR for day-time can be boosted. Laboratory simulations of off-beam lidar observations are currently underway (Davis et al., 1998) and new field experiments are in the planning stages.

Acknowledgments. This work was supported by the Environmental Sciences Division of U.S. Department of Energy (grant DE-A105-90ER61069 to NASA's Goddard Space Flight Center) as part of the Atmospheric Radiation Measurement (ARM) program and by LANL's Laboratory Directed Research & Development (LDRD) program via the Remote Sensing Science (RSS) thrust. We thank Drs. Daniel Cooper, Edwin Eloranta, Pierre Flamant, Aimé Fournier, Sigfied Gerstl, Cheng Ho, Alexander Marshak, Harvey Melfi, Robert Menzies, Jacques Pelon, David Winker, and Warren Wiscombe for fruitful discussions.

References

Cahalan, R.F., Bounded cascade clouds: Albedo and effective thickness. *Nonlinear Processes in Geoph., 1*, 156–167, 1994.

Case, K.M. and Zweifel, P.F., *Linear transport theory*, Addison–Wesley, Reading (Mass), 1967.

Clothiaux, E.E., Miller, M.A., Albrecht, B.A., Ackerman, T.P., Verlinde, J., Babb, D.M., Peters, R.M., and Syrett, W.J., An evaluation of a 94-GHz radar for remote sensing of cloud properties, *J. Atmos. and Oceanic Technol., 12*, 201–229, 1995.

Davis, A. and Marshak, A., Cloud responses from cw and pulsed lasers as Green's functions: What do they tell us? & Can we measure them? In *8th International Worskshop on MUltiple SCattering Lidar Experiments (MUSCLE 8 – Extended Abstract Volume)*, March 04–06, 1996, Québec (Qc), pp. 67–71, Def. Res. Est.Valcartier (DREV), 1996.

Davis, A., Winker, D.M., Marshak, A., Spinhirne, J.D., Cahalan, R.F., Love, S.P., Melfi, S.H., and Wiscombe, W.J., Retrieval of physical and optical cloud thicknesses from space-borne and wide-angle lidar, in *Advances in Atmospheric Remote Sensing with Lidar*, Eds. Ansmann, A., et al., Springer-Verlag, Berlin, pp. 193–196, 1997a.

Davis, A., Marshak, A., Cahalan, R.F., and Wiscombe, W. J., The LANDSAT scale-break in stratocumulus as a three-dimensional radiative transfer effect, implications for cloud remote sensing, *J. Atmos. Sci.*, *54*, 241–260, 1997b.

Davis, A., Spinhirne, J.D., McGill, M., and Cahalan, R.F., Off-beam cloud lidar: First detection of diffusing photons, in *Proceedings of Winter Topical Meeting on "Optical Remote Sensing of the Atmosphere"*, February 10–14, 1997, Santa Fe (NM), Optical Society of America, Washington (DC), pp. 39–41, 1997c.

Davis, A.B. and Cahalan, R.F., Off-beam (multiply-scattered) lidar returns from stratus, 1: Cloud-information content & sensitivity to noise, in *19th International Laser Radar Conference Proceedings*, Eds. Singh, U., Ismail, S., and Schwemmer, G., NASA Center for Aero-Space Information (CASI), Greenbelt (Md), pp. 91–94, 1998.

Davis, A.B., Ho, C., and Love, S.P., Off-beam (multiply-scattered) lidar returns from stratus, 2: Space-time measurements in a laboratory simulation, iin *19th International Laser Radar Conference Proceedings*, Eds. Singh, U., Ismail, S., and Schwemmer, G., NASA Center for Aero-Space Information (CASI), Greenbelt (Md), pp. 55–58, 1998.

Flesia, C. and Schwendimann, P. (Eds.), Special section on MUltiple SCattering in Lidar Experiments (MUSCLE). *Applied Physics B – Lasers and Optics*, *B60*, pp. 315–362, 1995.

Ivanova, K. and Ackerman, T., Multifractal characterization of liquid water in clouds, *Phys. Rev. E*, 1998 (in press).

King, M.D., Radke, L.F., and Hobbs, P.V., Determination of the spectral absorption of solar radiation by marine stratocumulus clouds from airborne measurements within clouds. *J. Atmos. Sci.*, *47*, 894–907, 1990.

Kornreich, D.E. and Ganapol, B.D., Numerical evaluation of the three-dimensional searchlight problem in a half-space, *Nucl. Sci. Eng.*, *127*, 317–337, 1997.

Marshak, A., Davis, A., Cahalan, R., and Wiscombe, W., Bounded cascade models as nonstationary multifractals. *Phys. Rev.*, *E49*, 55–69, 1994.

Marshak, A., Davis, A., Wiscombe, W., & Cahalan, R., Radiative smoothing in fractal clouds, *J. Geophys. Res.*, *D100*, 26247–26261, 1995.

Marshak, A., Davis, A., Cahalan, R.F., and Wiscombe, W.J., Nonlocal Independent Pixel Approximation: Direct and inverse problems, *IEEE Trans. Geosc. and Remote Sens.*, *36*, 192–205, 1998.

McGill, M.J., Marzouk, M., Scott, V.S., and Spinhirne, J.D., Holographic circle-to-point converter with particular applications for lidar work, *Opt. Eng.*, *36*, 2171–2175, 1997.

Miller, S.D. and G.L. Stephens: Multiple scattering effects in the lidar pulse stretching problem, *J. Geophys. Res. – D*, 1998 (in press).

Pfeilsticker, K.P., Erle, F., Funk, O., Veitel, H., and Platt, U., First geometrical pathlength distribution measurements of skylight using the oxygen A–band absorption technique, I: Measurement technique, atmospheric observations, and model calculations, *J. Geophys. Res. – D*, 1998 (in press).

Platt, C.M. et al. (27 authors), The Experimental Cloud LIdar Pilot Study (ECLIPS) for cloud radiation research, *Bull. Amer. Meteor. Soc.*, *75*, 1635–1654, 1994.

Priedhorsky, W.C., Smith, R.C., and Ho, C., Laser ranging and mapping with a photon-counting detector, *Appl. Opt.*, *35*, 441–452, 1996.

Stephens, G.L. and A. Heidinger, Molecular line absorption in a scattering atmosphere: I Theory, *J. Atmos. Sci.*, *54*, 1998 (accepted).

van de Hulst, H.C., *Multiple light scattering: Tables, formulas, and applications*. 2 Vols., Academic Press, San Diego (Ca), 1980.

Winker, D.M., Simulation and modeling of the multiple scattering effects observed in LITE data, in *Advances in Atmospheric Remote Sensing with Lidar*, Eds. Ansmann, A., Neuber, R., Rairoux, P., and Wadinger, U., Springer-Verlag, Berlin, pp. 185–188, 1996.

Winker, D.M., Couch, R.H. and McCormick, M.P., An overview of LITE: NASA's Lidar In-space Technology Experiment., *Proc. IEEE*, *84*, 164–180, 1996.